A Numerical Study on Liquefaction Induced Settlements by Using PM4Sand Model

A Numerical Study on Liquefaction Induced Settlements by Using PM4Sand Model

Ozan Subasi [1,2], Serdar Koltuk [3], Merve Akbas [2], Recep Iyisan [2]

[1] Department of Civil Engineering, Turkish-German University, Istanbul, Turkey

[2] Department of Civil Engineering, Istanbul Technical University, Istanbul, Turkey

[3] HPC AG The Engineering Company, Stuttgart, Germany

subasi@tau.edu.tr/subasio@itu.edu.tr

Abstract: Abstract: The destructive effects of earthquakes negatively affect many people's lives and cause a large number of lives and property losses. One of the most crucial factors that increase the destructive effects and structural damages of earthquakes is the deformations in the soil layers during strong ground motion. Especially liquefaction due to sudden increase in pore water pressure during strong ground motion in saturated sandy soils causes large deformations in the soil layers; hence leads to severe damage to the structures. Therefore, it is necessary to determine the liquefaction-induced deformations and settlements in the soil layers with high liquefaction potential. Following this purpose, three different two-dimensional fully saturated soil profiles with 35, 55, 75 % relative densities were created and carried out by using different strong ground motions for estimation of liquefaction-induced free field settlements. The finite element code "Plaxis 2D" and constitutive model "PM4Sand" were used in the analysis. The results of finite element (FE) analyses were compared with semi-empirical methods in the literature. The liquefaction state observed with pore pressure ratio (R_u) and safety factor (FS) is similar in numerical and empirical methods. The FE analyses have shown that the evaluation of free-field, liquefaction-induced settlements obtained from PM4Sand-Model have considerably lower settlement values than the semi-empirical methods. However, the semi-empirical method suggested by Cetin et al. (2009) and numerical analyses gave quite similar settlement results to each other. Moreover, there is no direct relationship between the liquefaction-induced settlements and the earthquake source properties in the numerical method. However, this is different for semi-empirical methods, and there is a relationship between strong ground motion features and liquefaction-induced settlements.

1. Introduction

During an earthquake, the seismic waves move between the soil layers from the source to the surface, and this causes ground shaking. The effects of a strong ground motion appear in different ways, such as structural damages, foundation and slope failures, and soil liquefaction. One of the most significant factors that increase an earthquake's destructive effect is the cyclic shear strain in the soil layers during strong ground motion. Especially in fully saturated sand layers, liquefaction-induced settlement is observed due to the sudden increase in pore water pressure during strong ground motion. For this reason, the estimation of liquefaction-induced settlements plays a critical role in the stability and serviceability of foundation systems.

Many fields, experimental and model studies have been carried out on the liquefaction phenomenon and consequences of liquefaction. In the laboratory, using cyclic triaxial test and dynamic simple shear devices series of experiments were carried out for different relative densities, the concept of liquefaction, and the parameters affecting liquefaction [1, 2, 3, 4]. The model experiments were carried out to observe liquefaction and pore pressure dissipation [5, 6, 7]. After Loma Prieta and Christchurch earthquake, field investigations were carried out to observe the consequences of liquefaction, such as liquefaction-induced settlement and sand boiling [8, 9, 10, 11, 12].

The pore water pressure increases in the saturated sand soil layer during the earthquake. With this increase in pore pressure, soil strength decreases, and liquefaction is observed when the pore water pressure is equal to the effective stress. After liquefaction, excess pore water pressures dissipate and liquefaction induced settlements observed on the soil surface. Some researchers have focused on this result of liquefaction for determining free field liquefaction-induced settlements. Some semi-empirical methods developed based on laboratory testing calibrated by using data obtained from the field cases [13, 14, 15, 16, 17]. With the development of computational tools and advanced constitutive models, numerical methods have become popular in predicting liquefaction-induced settlements for complex ground, drainage, and load conditions [18, 19, 20, 21].

This study aims to estimate the free field liquefaction-induced settlements using two-dimensional fully coupled finite element (FE) analyses. The dynamic behavior of the soil under earthquake loading is modeled by using PM4Sand. Sand layers are prepared with three different relative densities, 35%, 55%, 75%, and five different strong ground motions are used in the numerical analyses. The results of the FE analyses are compared with those obtained from well-known, semi-empirical methods proposed by Wu et al. (2003) and Cetin et al. (2009) [16,17].

2. Numerical study

Within this study's scope, two-dimensional soil profiles with a relative density of 35, 55, and 75 % were created, and liquefaction-induced settlements for free field conditions were examined with PM4Sand constitutive model in the Plaxis 2D 2019 finite element software. The modeling approach is given in the following parts.

2.1. Seismic input

Five different real earthquake acceleration-time histories recorded on rock-outcrop are used in the FE analyses [22]. The choice of these records is motivated by the fact that they are characterized by substantially different fault mechanisms, fundamental frequencies (f_{eq}), moment magnitudes (M_w), arias intensities (I_a), time (T), and peak ground acceleration (PGA) on the rock outcrop. The features of using earthquakes are given in Table 1.

Table 1. Strong ground motion parameters of input earthquakes [22].

No	Earthquakes	Fault Mechanism	Time (s)	M_w	PGA (g)	f_{eq}(Hz)	I_a (m/s)
1	Hector Mine (USA)	Strike Slip	45.0	7.13	0.31	1.82	1.80
2	Kocaeli (Turkey)	Strike Slip	30.0	7.51	0.17	1.93	0.53
3	L'aquila (ITALY)	Normal	40.0	6.30	0.31	0.59	1.05
4	Loma Prieta (USA)	Reverse Oblique	40.0	6.93	0.56	2.69	1.63
5	Manjil (IRAN)	Strike Slip	53.5	7.37	0.53	2.93	4.31

These signals were baseline-corrected and bandpass filtered between 0.5-15 Hz according to the Butterworth filter type for compatibility with the numerical domain's mesh dimension. The filtered acceleration-time histories of input earthquakes are shown in Figure 1. The earthquake loading was inputted as a prescribed displacement along the base of the model in Plaxis. A value of 0.5 m was assigned to the x-component of the prescribed displacement, while the y-direction was fixed.

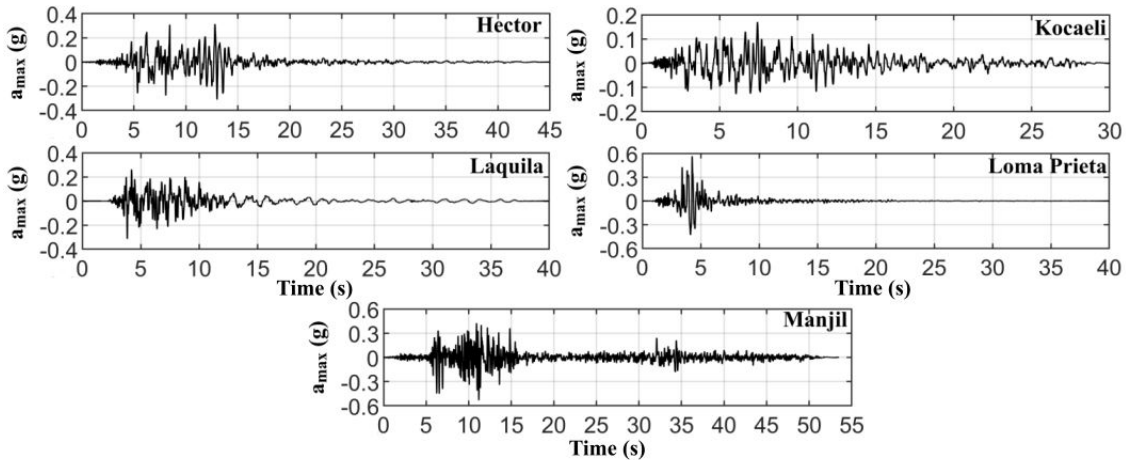

Figure 1. Acceleration-time histories of input earthquakes.

2.2. Two-dimensional numerical model

According to the past earthquakes, liquefaction has mainly occurred at depths less than approximately 20 m. Therefore, a 20 m thick, saturated sand layer was created by considering this underlain by a 1 m thick rock formation to apply strong ground motion to the soil profile. The groundwater table is located on the surface. The length of the model was chosen as 100 m, and a 1 m drained zone was defined on both sides to comply with boundary conditions. In the analyses, the bottom boundary condition was defined as "compliant base", while the upper and lateral boundaries were defined as "free-field". The soil profile used in the analysis is shown in Figure 2.

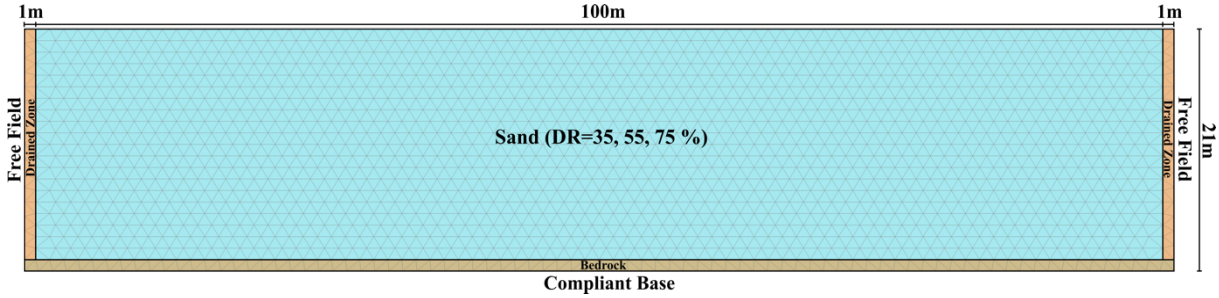

Figure 2. Numerical model.

In numerical analysis, mesh density significantly affects the results, especially in dynamic analysis. Therefore, choosing optimum mesh density allows both the analysis to be consistent and the model waves' correct propagation. The fact that redundant mesh density extends the analysis time and this is not an uneconomical solution. For this reason, Equation 1, which is widely used in dynamic analyses, was selected to determine the average element size. In this equation, $V_{S,min}$ is the lowest shear wave velocity in the soil layer, and f_{max} is the highest frequency of the input earthquake motion [23].

$$Average\ Element\ Size = V_{S,\min} / 8 f_{\max} \quad (1)$$

The critical time step must be limited according to Equation 2 to prevent waves from traveling through more than one element within one dynamic time step:

$$\Delta t \leq I_{\min} / V_{S,layer} \quad (2)$$

In Equation 2, I_{min} is the minimum length between two nodes of an element and $V_{s,layer}$ is the shear wave velocity of layer [24].

Based on the statement above, 3416 elements with 15-nodes with an average element size of 1.20 m were used. In addition to this, taking into account, the time step was determined as 0.005 in the dynamic analyses.

2.3. Constitutive model

PM4Sand constitutive model is a stress-ratio controlled, critical state compatible, bounding-surface plasticity model, for sands' liquefaction behavior [21, 25]. Although the PM4Sand model is adequate for liquefaction behavior, it is not sufficient in calculating the initial stress conditions [26]. Therefore, the Hardening Soil model with small-strain stiffness (HSS) is added to determine the initial stress conditions accurately [27].

In this study, the Hardening Soil model with small-strain stiffness (HSS) was used for initial stress conditions, and PM4Sand was used for the liquefaction behavior of the clean Ottawa Sand. PM4Sand and HSS parameters for different relative densities are given in Table 2 [21, 27, 28].

Table 2. PM4Sand and HSS Parameters used in the numerical models [21, 27, 28].

PM4Sand				Hardening Small Strain			
Symbol	**D_R=35**	**D_R=55**	**D_R=75**	**Symbol**	**DR=35**	**DR=55**	**DR=75**
γ_{dry} (kN/m^3)	15.34	15.90	16.52	γ_{dry} (kN/m^3)	15.34	15.9	16.52
γ_{sat} (kN/m^3)	19.36	19.71	20.10	γ_{sat} (kN/m^3)	19.36	19.71	20.1
e	0.695	0.635	0.575	e	0.695	0.635	0.575
D_{R0}	0.35	0.55	0.75	E_{50ref} (MPa)	21	33	45
G_0	476	677	890	E_{oedref} (MPa)	21	33	45
h_{p0}	0.53	0.4	0.63	E_{urref} (MPa)	63	99	135
e_{max}	0.8	0.8	0.8	m	0.59	0.53	0.47
e_{min}	0.5	0.5	0.5	c' (MPa)	0	0	0
P_a (MPa)	0.101	0.101	0.101	ϕ'(°)	33	33	33
n^b	0.5	0.5	0.5	$\gamma_{0.7}$	0.00017	0.00015	0.00013
n^d	0.1	0.1	0.1	G_{0ref} (MPa)	83.8	97.4	111
ϕ_{cv} (°)	33	33	33	υ	0.3	0.3	0.3
υ	0.3	0.3	0.3	P_{ref} (MPa)	0.1	0.1	0.1
Q, R	10 1.5	10 1.5	10 1.5	R_f	0.956	0.931	0.906

*γ_{dry}: dry unit weight, γ_{sat}: saturated unit weight, **e**: void ratio, D_{R0}: relative density, G_0: shear modulus coefficient, h_{p0}: contraction rate parameter, e_{max}, e_{min}: maximum and minimum void ratio, P_a: atmospheric pressure, n^b: bounding surface parameter, n^d: dilatancy surface parameter, ϕ_{cv}: critical state friction angle, υ: Poisson ratio, **Q, R**: Critical state line parameters, E_{50ref}: secant stiffness modulus, E_{oedref}: tangent stiffness modulus, E_{urref}: unloading reloading stiffness modulus, **m**: rate of stress dependency, **c'**: effective cohesion, ϕ': effective friction angle, $\gamma_{0.7}$: shear strain ratio, G_{0ref}: reference shear modulus at very small strains, P_{ref} : reference stress level, R_f: failure ratio*

Hysteretic damping of the soil model can capture damping at strains larger than 0.0001-0.01%, depending on material properties' values. Even at low deformation levels, the behavior of the soil is irreversible. It is suggested to define Rayleigh damping coefficients associated with a small damping ratio for sand layers, and this formulation is demonstrated by Eq. (3). In Eq. (3), the damping matrix C is given by a portion of the mass matrix M and a portion of the stiffness matrix K, as a function of the Rayleigh coefficients, α and β;

$$[C] = \alpha[M] + \beta[K] \tag{3}$$

In calculating these coefficients, two frequency variables, Target 1 (f_1) and Target 2 (f_2), are used in Plaxis. In the analysis f_1 shows the natural frequency of all soil layers and is calculated with Equation 4. In Equation 4, $V_{S,mean}$ is average shear wave velocity, and H is layer thickness.

$$f_1 = V_{S,mean} / 4H \tag{4}$$

Another parameter, f_2, represents the input earthquake motion (f_{eq}) ratio and the natural frequency of the soil (f_1) and is calculated by Equation 5. The f_2 obtained from Equation 5 is used in calculations by rounding it to the nearest odd number [24].

$$f_2 = f_{eq} / f_1 \tag{5}$$

In this study, analyses were made using 1, 2, and 3 % Rayleigh damping values, and the effects of different damping values on the results were investigated. The 2% Rayleigh damping value was used in analyses since no significant difference was observed in this investigation.

2.4. Analysis stages

The numerical analyses were carried out in four stages:

Stage 1: In the first stage, the initial stress field was established using the K_0 procedure.

Stage 2: The second stage was a plastic analysis in which an empty step was created by using Hardening Small Strain Model. The reason for creating this stage is that the PM4Sand model cannot adequately model the static condition [26].

Stage 3: The dynamic analysis was performed in the third stage by using the PM4Sand-Model. The drainage type chosen was Undrained A to generate the development of excess pore pressure. In this type of drainage, undrained behavior, effective strength, and stiffness parameters are observed in the analysis.

Stage 4: The dynamic analysis with consolidation was carried out to determine the settlements after liquefaction (post liquefaction-induced settlements). The PostShake parameter equal to 1, drainage type is drained, and no seismic loading was considered. At this stage, dynamic analysis with consolidation option based on Biot Theory (1956) is used. Because The Biot Theory is constructed on the theoretical model of consistent solid skeleton and a freely moving pore fluid. The constitutive equations give on the relationship between the strain and the stress [29]. In this way, the liquefaction-induced settlements can be estimated thanks to dynamic with consolidation option.

2.5. Results of finite element analysis

The liquefaction-induced settlements are calculated by using Plaxis. A liquefaction potential in the numerical analyses is expressed through the excess pore pressure ratio (R_u), representing the ratio of excess pore pressure to the initial vertical effective stress at a certain depth. In Figure 3, R_u values for the Kocaeli earthquake are illustrated as an example for different relative densities, and the points P1,

P2, P3, P4 were created to follow the change of excess pore water pressure during the strong ground motions.

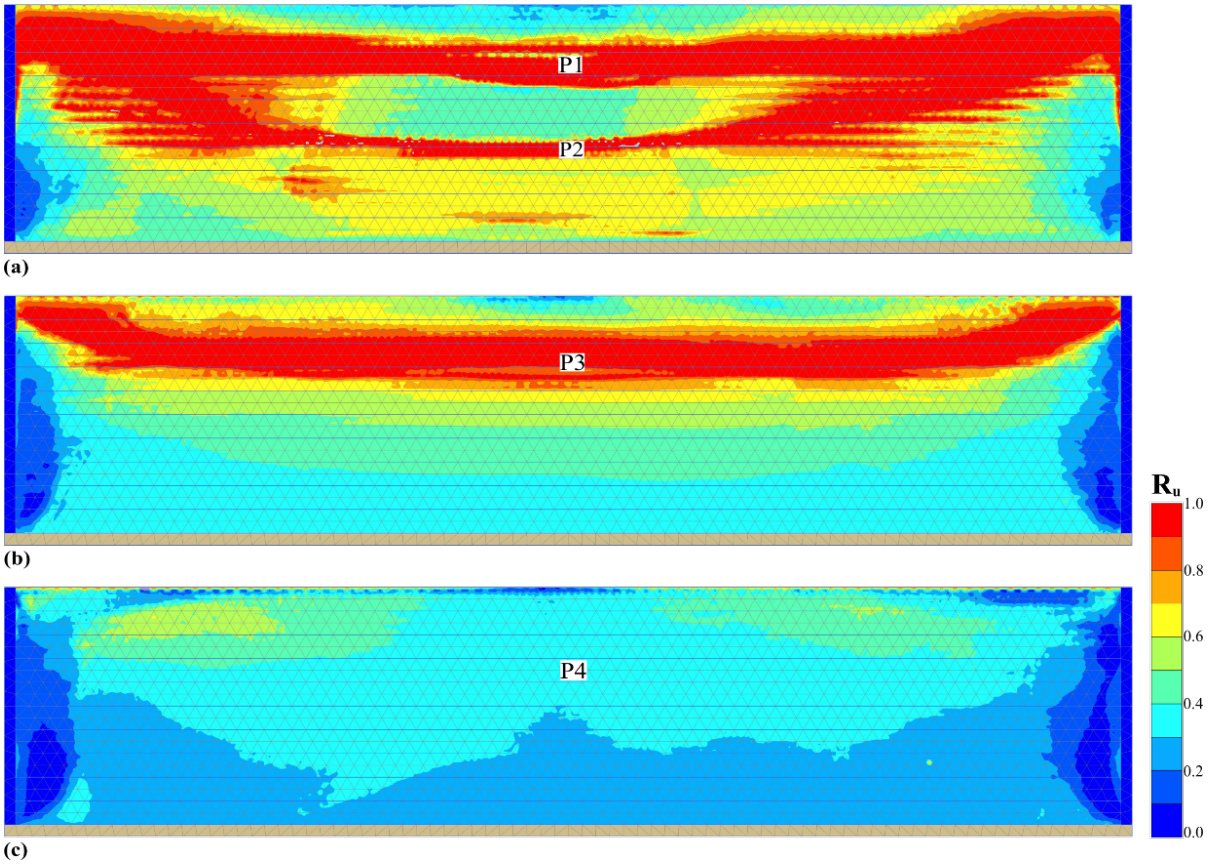

Figure 3. Results of excess pore pressure ratio (R_u) for a) D_R=35%, b) D_R=55%, c) D_R=75%.

The change of excess pore water pressure at the points P1, P2, P3, P4 is illustrated in Figure 4 for the Kocaeli earthquake. As seen in Figure 4, excess pore water pressure increased to a specific value during the strong ground motion depending on the depth. Then the pore water pressure dissipates and reaches zero over time. In this way, the liquefaction-induced settlements are determined according to the pore water pressure change.

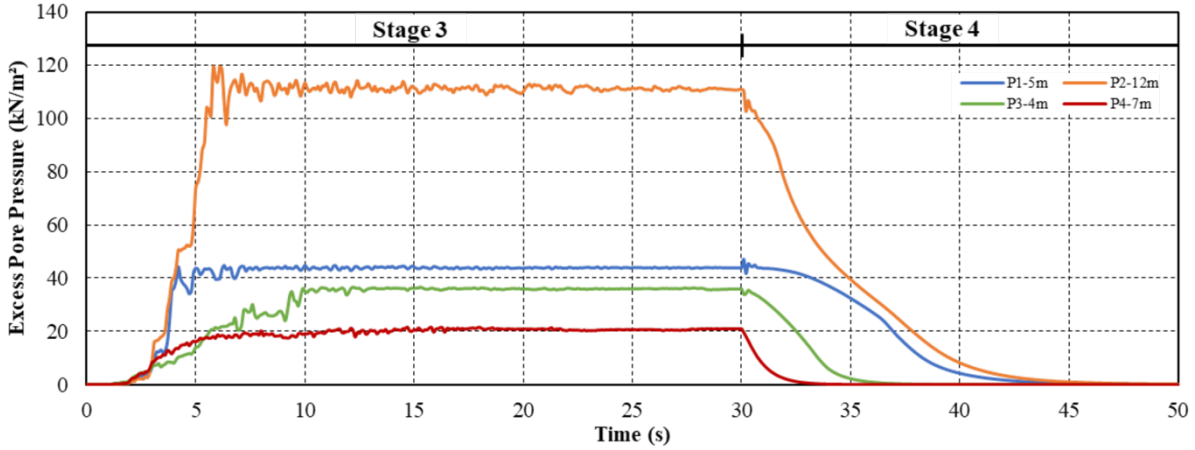

Figure 4. The change excess pore pressure with time for P1, P2, P3, P4.

As a result of the numerical analysis, liquefaction-induced settlements obtained for five different earthquakes are shown in Table 3. In this table, T_3 and T_4 show the duration of the strong ground motions for the 3rd and 4th phases, and S3 and S4 are the liquefaction-induced settlements at the end of the stages.

Table 3. Liquefaction status and liquefaction-induced settlements according to numerical analyses.

Earthquakes	M_w	PGA (g)	T (s)		D_R=35 %			D_R=55 %			D_R=75 %		
			T_3 (s)	T_4 (s)	R_u	S3 (m)	S4 (m)	R_u	S3 (m)	S4 (m)	R_u	S3 (m)	S4 (m)
Hector Mine	7.13	0.31	45.0	30.0	1	0.123	0.269	1	0.055	0.131	0	0.041	0.042
Kocaeli	7.51	0.17	30.0	20.0	1	0.015	0.073	1	0.019	0.039	0	0.020	0.021
L'aquila	6.30	0.31	40.0	30.0	1	0.034	0.180	1	0.026	0.076	0	0.024	0.026
Loma Prieta	6.93	0.56	40.0	20.0	1	0.046	0.144	1	0.029	0.051	0	0.015	0.016
Manjil	7.37	0.53	53.5	21.5	1	0.091	0.172	1	0.058	0.098	0	0.037	0.040

According to Table 3, liquefaction was observed in all soil profiles except D_R=75%, considering the R_u parameter. The maximum liquefaction-induced settlement was detected in the Hector Mine earthquake. This situation clearly shows no direct linear relationship between strong ground motion parameters and liquefaction-induced settlements. When the settlements obtained in the 3rd and 4th stages are compared, it is indicated that the majority of the liquefaction-induced settlements occur after strong ground motion. This situation is clearly shown in Figure 5. The change over time of settlements is shown for five different earthquakes and D_R=35 % in Figure 5.

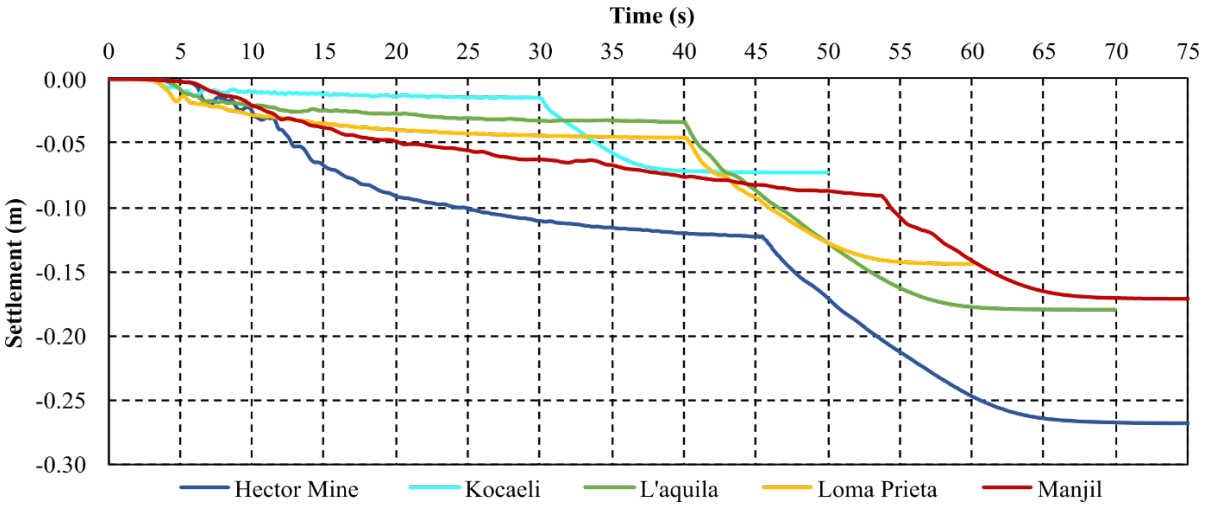

Figure 5. Change of liquefaction induced settlements with time for D_R=35%.

3. Comparison of the results of the finite element analyses and semi-empirical methods

In this study, the numerical analysis results were compared with the literature's current and semi-empirical correlations. The most up-to-date method used to determine liquefaction-induced settlements in free-field conditions was proposed by Cetin et al. (2009). They defined in terms of a maximum probability of liquefaction-induced straining for saturated clean sands. Their databases are based on cyclic laboratory test results and test results, including maximum shear and post-cyclic volumetric strains together with a number of stress cycles, relative density, and "index" test results. These test results were used for the development of probabilistically based post-cyclic strain correlations [17]. Another method used in this study was proposed by Wu et al. (2004). The post-liquefaction volumetric

strain is correlated to the cyclic stress ratio (CSR) and SPT-$N_{1,60}$ values based on the results of cyclic simple shear tests on clean sands [16].

Firstly, within the research scope, soil profiles compatible with numerical analysis were created to perform liquefaction analysis using the correlations suggested for the relationship between relative density and $N_{1,60}$ [30]. In liquefaction analysis, the earthquake load is determined with the soil column approach [31]. Therefore, these soil profiles were analyzed with DEEPSOIL V7, and maximum horizontal accelerations were obtained on the surface for use in liquefaction analysis [32]. By using these surface acceleration, liquefaction-induced settlements were determined according to Wu et al. (2003) and Cetin et al. (2009) with the help of Settle 3D software [16, 17, 33].

The liquefaction-induced settlements obtained by semi-empirical methods are shown in Table 4. a_{max} is the maximum surface acceleration performed in DEEPSOIL V7 and used in liquefaction analysis. In Table 4, S_{Wu} and S_{Cetin} are liquefaction-induced settlements calculated using the methods suggested by Wu et al. (2003) and Cetin et al. (2009), respectively. Furthermore, FS is the factor of safety coefficient, and liquefaction occurs less than 1.

Table 4. Liquefaction status and liquefaction-induced settlements as a result of empirical analyses.

Earthquakes	D_R =35 %				D_R =55 %				D_R =75 %			
	FS	a_{max} (g)	S_{Wu} (m)	S_{Cetin} (m)	FS	a_{max} (g)	S_{Wu} (m)	S_{Cetin} (m)	FS	a_{max} (g)	S_{Wu} (m)	S_{Cetin} (m)
Hector Mine	<1	0.090	0.821	0.220	<1	0.162	0.379	0.166	>1	0.222	0.000	0.000
Kocaeli	<1	0.069	0.753	0.164	<1	0.108	0.253	0.124	>1	0.118	0.000	0.000
L'aquila	<1	0.096	0.835	0.232	<1	0.159	0.257	0.149	>1	0.166	0.000	0.000
Loma Prieta	<1	0.110	0.873	0.255	<1	0.161	0.378	0.162	>1	0.269	0.000	0.000
Manjil	<1	0.116	0.885	0.263	<1	0.189	0.400	0.179	>1	0.220	0.000	0.000

In Table 4, liquefaction was observed in all analyses except for D_R=75%, and the maximum liquefaction induced-settlements occurred in the Manjil earthquake. This result shows a linear relationship between earthquake source characteristics and liquefaction-induced settlements in semi-empirical methods. In addition to that, liquefaction-induced settlements calculated with Wu et al. (2003) much higher than Cetin et al. (2009). However, the semi-empirical method suggested by Cetin et al. (2009) and numerical analyses gave quite similar settlement results to each other. Moreover, liquefaction calculated by both numerical and semi-empirical methods is similar. The maximum horizontal accelerations determined to calculate the earthquake load on the soil column increase with the relative densities.

4. Results and discussions

A series of fully-coupled, nonlinear, dynamic analyses were carried out to estimate liquefaction-induced free-field settlements using the finite element code “Plaxis 2D” with the PM4Sand-Model. In the analyses, a sand layer with three different relative densities of 35%, 55%, 75%, and five different strong ground motions was used. The results of the FE analyses were compared with those obtained from the well-known semi-empirical methods proposed by Wu et al. (2003) and Cetin et al. (2009).

The following results can be drawn from the analyses performed. The liquefaction state is similar in analyzes performed by both numerical and empirical methods. The liquefaction-induced settlements obtained by numerical methods are quite small compared to empirical methods. However, according to Cetin et al. (2009), liquefaction-induced settlements give an almost similar result to the numerical analysis. Moreover, there is no direct relationship between the liquefaction-induced settlements and the numerical method's earthquake source properties. Nevertheless, this is not the case for semi-empirical methods, and there is a relationship between strong ground motion features and liquefaction-induced

settlements. For this reason, earthquake source properties and liquefaction-induced settlements should be examined in more detail by numerical methods.

Acknowledgment(s)

Ozan Subası, who took part in this study, is supported by The Scientific and Technological Research Council of Turkey (TÜBİTAK) within the scope of the 2211-A National Ph.D. Scholarship Program.

References

[1] L. K. Chien, Y. N. Oh., and C. H. Chang, "Evaluation of liquefaction resistance and liquefaction induced settlement for reclaimed soil," *In Twelfth World. Conf. on Earthquake Eng*., 2000.
[2] S. Kim, & K. Park, "Proposal of liquefaction potential assessment procedure using real earthquake loading," *KSCE Journal of Civil Engineering*, 12(1), 15-24, 2008.
[3] S. S. Kumar, A. Dey, and A. M. Krishna, "Liquefaction Potential Assessment of Brahmaputra Sand Based on Regular and Irregular Excitations Using Stress-Controlled Cyclic Triaxial Test," *KSCE Journal of Civil Engineering*, 1-13, 2020
[4] E. E. Bayat, &, D. B. Gulen, "Undrained Dynamic Response of Partially Saturated Sands Tested in a DSS-C Device" *Journal of Geotechnical and Geoenvironmental Engineering*, 146(11), 04020118, 2020.
[5] O. Adamidis, G. S. P. Madabhushi, "Experimental investigation of earthquake–induced liquefaction in loose and dense sand layers," *SECED Young Engineers Conference*, 2013.
[6] N. Ecemis, "Simulation of seismic liquefaction: 1-g model testing system and shaking table tests," *European Journal of Environmental and Civil Engineering*, 17(10), 899-919, 2013
[7] J. Ramirez, A. R. Barrero, L. Chen, S. Dashti, A. Ghofrani, M. Taiebat, and P. Arduino, "Site response in a layered liquefiable deposit: evaluation of different numerical tools and methodologies with centrifuge experimental results," *Journal of Geotechnical and Geoenvironmental Engineering*, 144(10), 04018073, 2018.
[8] R. B. Seed, F. M. Riemer and, E. S. Dickenson "Liquefaction of Soils in the 1989 Loma Prieta Earthquake," *International Conferences on Recent Advances in Geotechnical Earthquake Engineering and Soil Dynamics*, 1991.
[9] K. Adalier, "Mitigation of earthquake induced liquefaction hazards," PhD Thesis, *Department of Civil Engineering, Rensselaer Polytechnic Institute*, Troy, NY, 1996.
[10] R. W. Boulanger, L. H. Mejia, & I. M. Idriss, "Liquefaction at moss landing during Loma Prieta earthquake," *Journal of Geotechnical and Geoenvironmental Engineering* 123(5), 453-467. 1997.
[11] M. Cubrinovski, J.D. Bray, M. Taylor, S. Giorgini, B. Bradley, L. Wotherspoon, and J. Zupan, "Soil liquefaction effects in the central business district during the February 2011 Christchurch earthquake," *Seismological Research Letters*, 82(6), 893-904, 2011.
[12] J. Bray, M. Cubrinovski, J. Zupan, and M. Taylor, "Liquefaction effects on buildings in the central business district of Christchurch," *Earthquake Spectra*, 30(1), 85-109, 2014.
[13] K. Tokimatsu, and Seed, H. B. Seed, _. "Simplified procedures of the evaluation of settlements in clean sands." *Rep. No. UCB/GT-84/16, Univ. of California, Berkeley*, 1984.
[14] K. Ishihara and M. Yoshimine, "Evaluation of settlements in sand deposits following liquefaction during earthquakes," *Soils and Foundations*, 32(1), 173-188, 1992.
[15] Y. Shamoto, J. M. Zhang, and K. Tokimatsu, "New charts for predicting large residual post-liquefaction ground deformation," *Soil Dynamics and Earthquake Engineering*, 17(7-8), 427-438, 1998.
[16] J. Wu, R. B. Seed, and J.M. Pestane, "Liquefaction triggering and post liquefaction deformations Montery 0/30 Sand under Uni-Directional Cyclic Simple Shear Loading". *Geotechnical Engineering Research Report, University of California,* 2003.

[17] K. O. Cetin, H. T. Bilge, J. Wu, A. M. Kammerer, R. B. Seed, "Probabilistic model for the assessment of cyclically induced reconsolidation (volumetric) settlements." *ASCE Journal of Geotechnical and Geoenvironmental Engineering,* 135(3), pp. 387- 398, 2009.
[18] D.S. Liyanapathirana, H.G. Poulos, "A numerical model for dynamic soil liquefaction analysis," *Soil Dynamics and Earthquake Engineering*, 22(9-12): 1007-1015, 2002.
[19] P.M. Byrne, S.S. Park, P. Beaty, M. Sharp, L. Gonzalez, T. Abdoun, "Numerical modeling of liquefaction and comparison with centrifuge tests," *Canadian Geotechnical Journal*, 41(2): 193-211, 2004.
[20] C. Chen and J. Zhang, "Constitutive modeling of loose sands under various stress paths," *International Journal of Geomechanics*, Vol. 13, No. 1, pp. 1-8 2013.
[21] R.W. Boulanger, K. Ziotopoulou, "PM4Sand (version 3.1 Revised Jully 2018): A sand plasticity model for earthquake engineering applications," *Report No. UCD/CGM-17/01, Center for Geotechnical Modeling, Department of Civil and Environmental Engineering*, University of California, Davis, CA, 2017.
[22] PEER, "*Pacific Earthquake Engineering Research Center Ground Motion Database*" https://ngawest2.berkeley.edu/site, 2020.
[23] R. L. Kuhlemeyer, and J. Lysmer, "Finite element method accuracy for wave propagation problems," *Journal of the Soil Mechanics and Foundations Division*, 99(5), 421-427, 1973.
[24] R.B.J. Brinkgreve, S. Kumarswamy and W.M. Swolfs, "Plaxis 2D Manuals" *Plaxis BV, Delft*, 2019.
[25] Y.F. Dafalias and M. Manzari, "Simple plasticity sand model accounting for fabric change effects," *Journal of Engineering Mechanics* 130(6): 622-634, 2004.
[26] G. Vilhar, R.B.J. Brinkgreve, L. Zampich "The PM4Sand Model 2018," *Plaxis BV, Delft*, 2018.
[27] R.B.J. Brinkgreve, E. Engin, H.K. Engin, "Validation of empirical formulas to derive model parameters for sands. In: Numerical methods in geotechnical engineering," *1 st Edition. CRC Press*, 137-142, 2010.
[28] A.M.P. Bastidas "Ottawa F-65 sand characterization". Ph.D Thesis, *University of California, Davis,* 2016.
[29] M.A. Biot, "General solutions of the equations of elasticity and consolidation for porous material," *Journal of Applied Mechanics*, 23(2), 1956.
[30] I.M. Idriss and R.W. Boulanger, "Soil liquefaction during earthquakes," *Earthquake Engineering Research Institute*, 2008.
[31] H. B. Seed, and I. M. Idriss, "Simplified Procedure for Evaluating Soil Liquefaction Potential", *Journal of the Soil Mechanics and Foundations Division,* Vol.97, 1971.
[32] Y.M.A. Hashash, M.I. Musgrove, J.A. Harmon, O. Ilhan, G. Xing, O. Numanoglu, D.R. Groholski, C.A., Phillips, and D. Park, "DEEPSOIL 7.0, User Manual". *Urbana, IL, Board of Trustees of University of Illinois at Urbana-Champaign,* 2020
[33] Rocscience Inc., "Settle3D settlement and consolidation analysis theory manual," *Toronto: Rocscience* 2009.